SEISMIC PERFORMANCE OF RC BRIDGE COLUMNS SUBJECTED TO BILATERAL EXCITATION

by

Kazuhiko Kawashima[1], Gakuho Watanabe[2] and Ryoji Hayakawa[3]

ABSTRACT

This paper represents a series of cyclic loading test and a fiber element analysis to clarify the effect of bilateral loading of reinforced concrete bridge columns. Four loading orbits (diagonal, square, circular and ellipsis) were used in the test in addition to the unilateral loading. It was found that an extensive deterioration of flexural strength and displacement ductility capacity occurs under the bilateral loading, and that the fiber element analysis provides an accurate simulation for the test results.

KEYWORDS: Bridges, Seismic Design, Reinforced Concrete Structures, Flexural Capacity, Ductility

1. INTRODUCTION

The combination of two lateral components of seismic effect has been a major concern in seismic design of bridges. It is obvious that during an earthquake a bridge is subjected to a set of three components of ground motions in two lateral and the vertical directions. Since the effect of vertical component is a unique problem, we have to consider a rational combination of two lateral components of seismic effect by appropriately taking account of the effect of vertical component.

In practice, it is general to size a bridge column assuming that it is subjected to two lateral components of a ground motion in the weak and strong axes independently. Flexural strength and ductility capacity of a column are generally determined based on the experimental data of cyclic loading test under unilateral direction. Since it has been revealed that flexural strength and ductility capacity under bilateral excitation are less than those under unilateral excitation, it is likely that the current design values for flexural strength and ductility capacities are overestimated

It was important to simplify design procedure when an analytical tool was poor. However, an improvement of design tools has made it possible to take account of the bilateral excitation effects in design. This is particularly important to non-standard bridges in which bilateral excitation effect is significant. It is required to properly include the effect of bilateral excitation effect in seismic design of bridges.

This paper presents a cyclic loading test for 5 reinforced concrete specimens with the same structural properties to clarify the effect of bilateral excitation. Accuracy of a fiber element analysis which includes a new empirical stress vs. strain relation of confined concrete is verified based on the test data.

2. EXPERIMENTAL SETUP

2.1 Experimental Models

Five reinforced concrete specimens with the same structural properties as shown in Fig. 1 were constructed. They are 1,750 mm tall and the effective column height is 1,350 mm. They were designed in accordance with the Japanese 1996 Design Specifications of Highway Bridges using the Type-I (middle-field) and Type-II (near-field) ground motions. Moderate ground condition (Type-II Ground Condition) was assumed. Axial stress at the plastic hinge region of the columns resulted from the dead weight of a superstructure was assumed 1 MPa.

[1] Professor, Department of Civil Engineering, Tokyo Institute of Technology, O-Okayama, Meguro, Tokyo, Japan 152-8552

[2] Research Associate, ditto

[3] Graduate Student, ditto

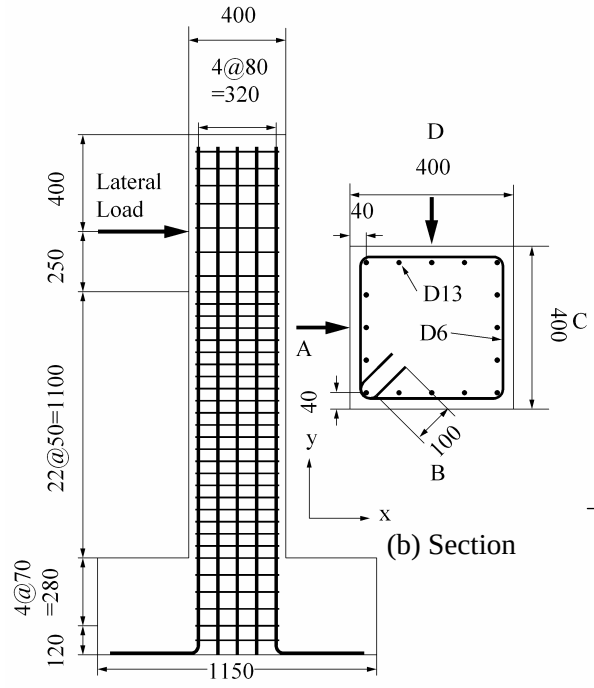

(a) Side (b) Section

Fig.1 Models

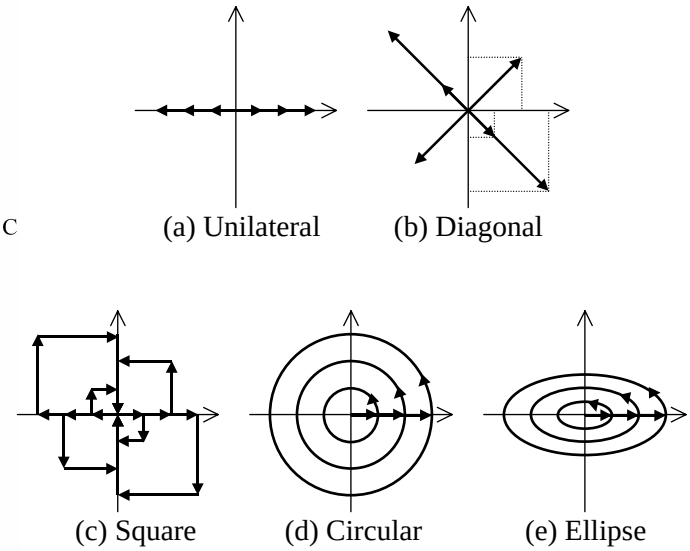

Fig. 2 Bilateral Orbits

Sixteen 13 mm diameter deformed bars with a nominal strength of 295 MPa (SD295A) were provided for longitudinal reinforcements, and 6 mm diameter deformed bars (SD295A) were provided every 500 mm interval for ties. The tie bars were anchored using 135 degree bent hooks with a development length of 100 mm. Longitudinal reinforcement ratio is 1.27 % and the tie volumetric reinforcement ratio is 0.79 %. Concrete strength ranged from 26.2 to 31.3 MPa.

2.2 Loadings

Cyclic loading test was conducted at the Tokyo Institute of Technology. Three dynamic actuators were used to provide bilateral loading under a constant vertical load of 160 kN. The vertical load resulted in an axial stress of 1 MPa at the plastic hinge region. In the following, the surfaces perpendicular to x axis are called A and C, while the surfaces perpendicular to y axis are called B and D, as shown in Fig. 1.

Four orbits as shown in Fig. 2 were used for the bilateral loading. In the diagonal loading, a column was first loaded three times in the diagonal direction in the 1st and 3rd quadrants with a displacement of u equivalent to 0.5 % drift. Then it was loaded three times in the diagonal direction in the 2nd and 4th quadrants with a displacement u equivalent to 1 % drift. This set of loading was repeated until failure. The loading displacement was step wisely increased from 0.5 % drift with an increment of 0.5 % drift. Since 1 % drift is 13.5 mm, it corresponds to approximately 3 times the yielding displacement u_y. Due to limitation of space, the loading test using the ellipsis orbit is not presented here.

In the square orbit loading, a column was first loaded in the x direction, and then in the y direction with a displacement of 0.5% drift keeping the displacement in the x direction. Then, the column was unloaded in the x direction first followed by unloading in the y direction to return to the rest position. This completes a loading with 0.5% drift in the 1st quadrant. The same loading was repeated in the 3rd quadrant. This loading in the 1st and 3rd quadrants were repeated three times. Then this set of loading was conducted in the 2nd and 4th quadrants by increasing the loading

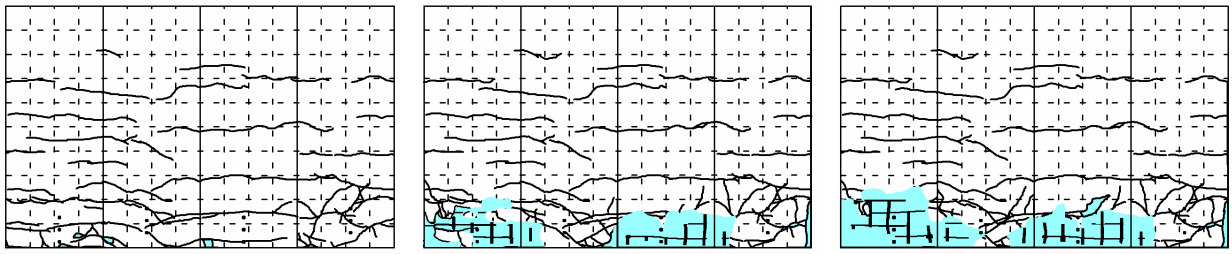

(a) Drift3.5% (b) Drift 4.0% (c) Drift 4.5%

(1) Unilateral (P-1)

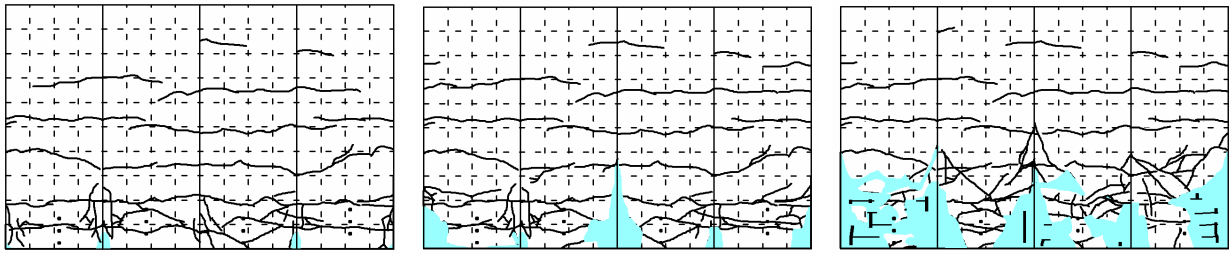

(a) Drift 2.0% (b) Drift 2.5% (c) Drift 3.5%

(2) Diagonal (P-2)

Fig. 3 Progress of Failure of Columns subjected to Unilateral and Diagonal Orbit Loadings

displacement to 1 % drift. Thus, loading was repeated alternatively in the 1st and 3rd quadrants and 2nd and 4th quadrants by increasing the loading displacement with an increment of 0.5 % drift.

In the circular orbit loading, a column was first loaded in the x direction until the displacement reaches 0.5% drift. From this point the column was loaded three times by circular orbit. Finally the column was unloaded in the x direction to the rest position. This set of loading was repeated until failure with an increment of loading displacement of 0.5 % drift.

For comparison, a column was loaded in the unilateral direction. Loading was repeated three times each and the loading displacement was step wisely increased from 0.5 % drift with an increment of 0.5 % drift.

3. PERFORMANCE OF COOLUMNS

3.1 Unilateral and Diagonal Loadings

Fig. 3 shows the progress of failure under the unilateral and diagonal orbit loadings. Under the unilateral loading, compression failure started to occur in the covering concrete in the plastic hinge zone at 3 % drift at A surface. At 4 % drift, the covering concrete started to spall off and longitudinal and tie bars were exposed. Some longitudinal bars buckled. The damage further progressed at 5 % drift.

Fig. 4 shows the lateral force vs. lateral displacement hysteresis under the unilateral loading. Hystereses under the diagonal loading which will be described latter are presented here for comparison. The hysteresis under the unilateral loading reaches at its maximum strength of 119.8 kN at 3 % drift, and is stable until 3.5 % drift. At 4 % drift, strength starts to deteriorate resulted from compression failure of the concrete and buckling of longitudinal bars. The strength deteriorates from its maximum strength by 37 % and 52 % at drift 4.5 % and 5 %, respectively.

On the other hand, the column subjected to the diagonal loading started to suffer damage at corners. For example, the column suffered damage at the corner of A and D surfaces (referred hereinafter A-D corner) and the corner of B and C surfaces (referred B-C corner) at 2.5 % drift, since the column was subjected to a diagonal loading in the direction of A-D and

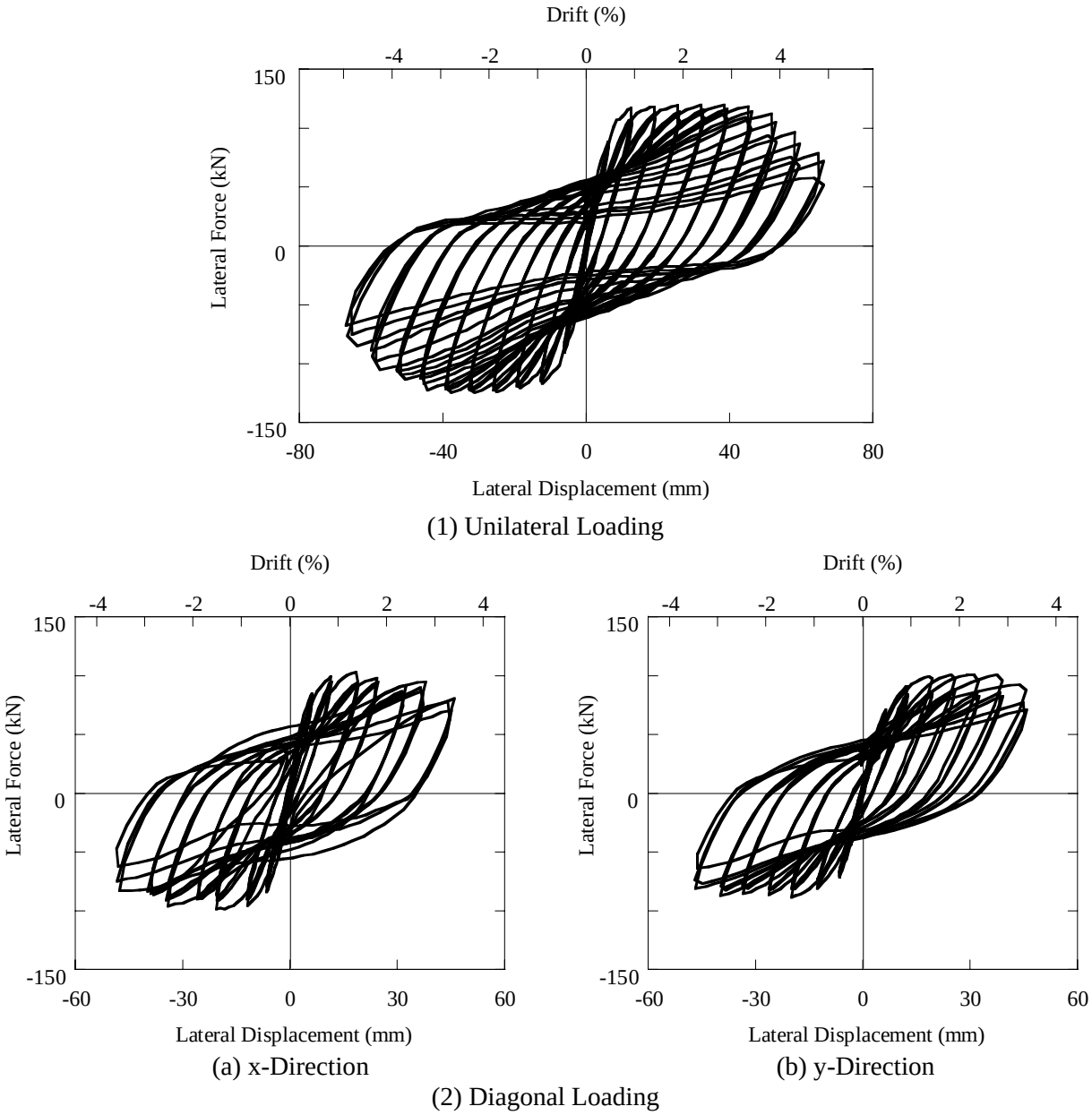

Fig. 4 Lateral Force vs. Lateral Displacement Hystereses of Columns subjected to Unilateral and Diagonal Loadings

B-C corners in this loading step. Similarly at 3 % drift, damage occurred at A-B and C-D corners since the column was loaded in this direction. Failure at the corners progressed to four surfaces, and the covering concrete spalled off all around the surfaces at 3.5 % drift. A couple of longitudinal bars buckled. The damage of the column under the diagonal loading is more extensive than that under the unilateral loading.

Fig. 4 (2) shows the lateral force vs. lateral displacement hystereses of the column subjected to the diagonal loading. The column reached its maximum strength of 103 kN at 1.5 % drift in the x direction, while it reaches its maximum strength of 100.6 kN at 2 % drift in the y direction. The strength deteriorated to 80 % of the maximum at 1st and 2nd excursion of 3.5 % drift loading in the x and y directions, respectively.

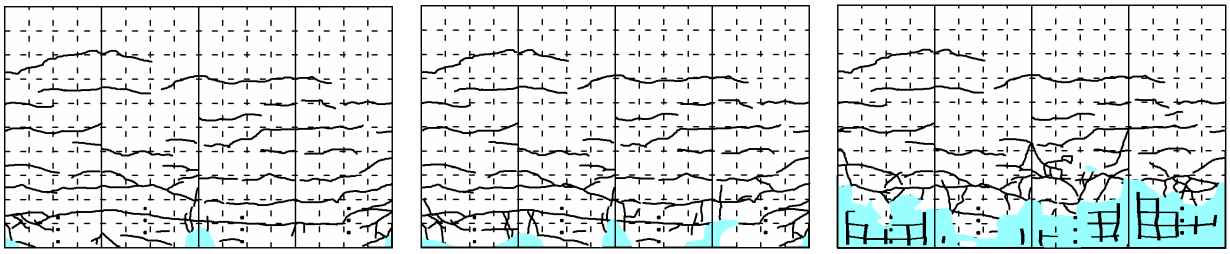

(a) Drift 2.0% (b) Drift 2.5% (c) Drift 3.5%

Fig. 5 Progress of Failure of a Column subjected to Square Orbit Loading

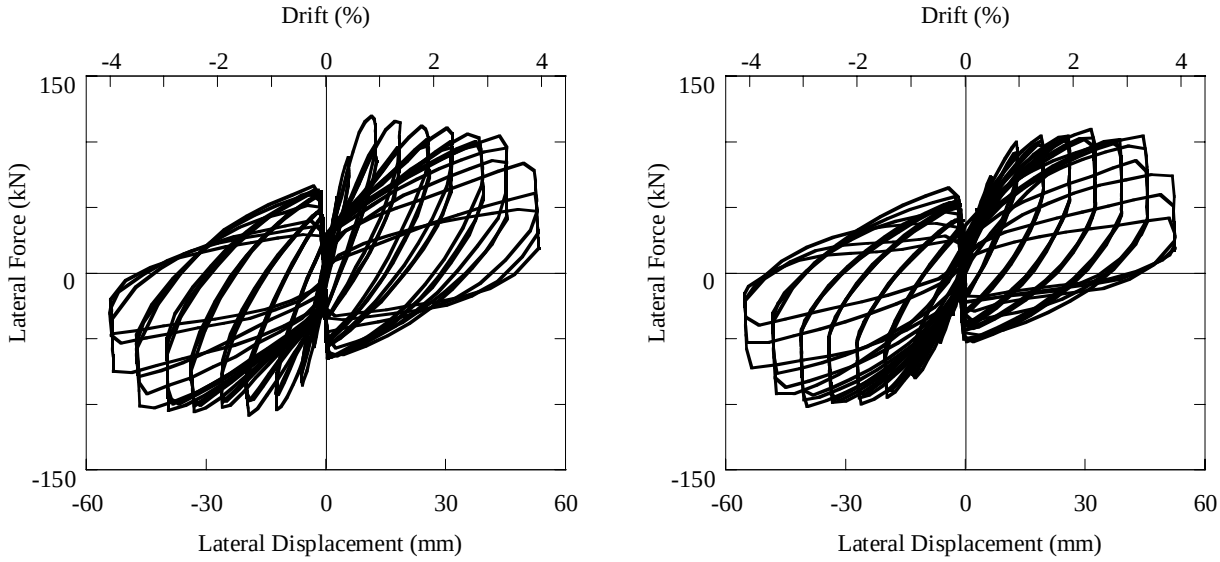

(a) x-Direction (b) y-Direction

Fig. 6 Lateral Force vs. Lateral Displacement Hystereses of Columns subjected to Square Orbit Loading

3.2 Square Orbit Loading

Fig. 5 shows progress of failure of the column subjected to the square orbit loading. Damage of the column under the square orbit loading was more extensive than the damage under the unilateral loading. Extensive failure occurred at A-B corner and C-D corner at 2.5 % drift. Longitudinal bars were partly exposed. At 3.5 % drift, not only the spalling off of the covering concrete at surfaces A, C and D in the range of 200-300 mm from the bottom, the core concrete suffered extensive damage. Longitudinal and tie bars were exposed. At 4 % drift, lateral confinement was lost, and longitudinal bars buckled at several heights in various directions.

Fig. 6 shows the lateral force vs. lateral displacement hystereses in x and y directions. The hystereses are unique because they are pinched near zero displacement. Taking the hysteresis in x direction as an example, this occurs because an unloading of the column in y direction (to the rest position) following an unloaded in x direction (refer to Fig. 2) results in a deterioration of restoring force in x direction. In other words, a deterioration of restoring force in one direction occurs as a consequence of an unloading in the perpendicular direction. This represents an effect of the interaction of restoring force of a column.

In Fig. 6, the hysteresis in the x direction reaches its maximum strength of 120 kN at 1 % drift. The strength in this direction subsequently deteriorates until 3 % drift, where a sudden decrease of the restoring force to 80 % of its maximum strength occurs. At 3.5 % drift, the restoring force significantly decreases at 2nd and 3rd loading excursions. On the other hand, in the y direction, the restoring force reaches its

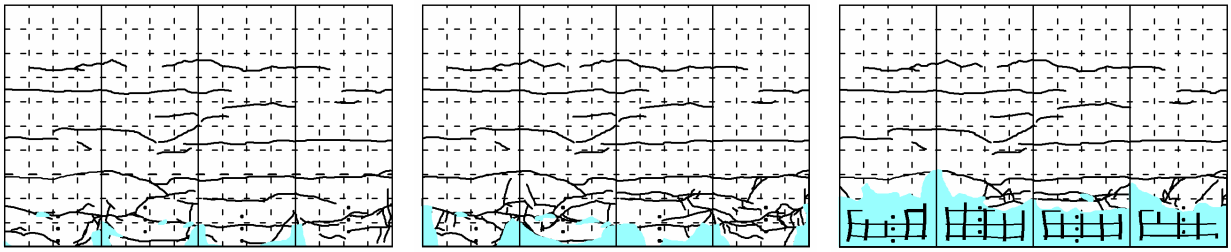

(a) Drift 2.0% (b) Drift 2.5% (c) Drift 3.5%

(1) Circular Loading (P-4)

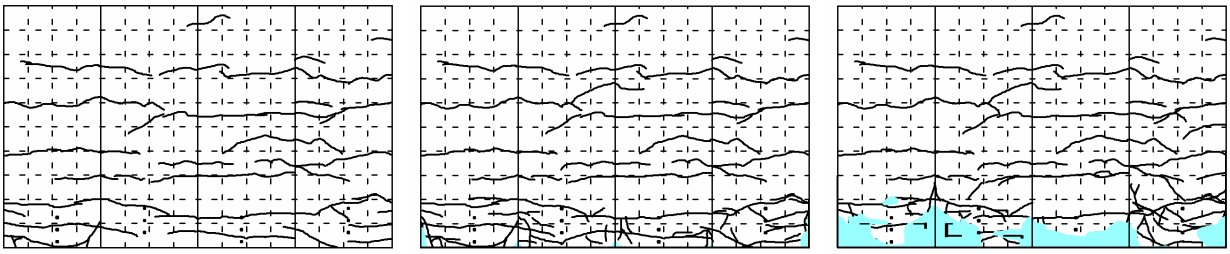

(a) Drift 2.0% (b) Drift 2.5% (c) Drift 3.5%

(2) Ellipse Loading (P-5)

Fig. 7 Progress of Failure of a Column subjected to Circular Orbit Loading

maximum strength of 109 kN at 2.5 drift. At 3.5 % drift, a sudden deterioration of the restoring force to 80 % of its maximum strength occurs.

3.3 Circular Orbit Loading

Fig. 7 shows progress of failure of the columns subjected to the circular orbit loading. Extensive damage similar to the damage under the square orbit loading occurs. Damage starts to occur at corners, and progressed to four surfaces at 2.5 drift. At 3.5 % drift, covering concrete completely spalled off up to about 200 mm from the bottom, and longitudinal and ties bars were exposed.

Fig. 8 shows hystereses of the columns under the circular orbit loading. The loading and unloading hystereses are round near the peak displacements. This results from the interaction of restoring force in two directions. Dislike the square orbit loading, the interaction of restoring occurs successively in the circular orbit loading. It is noted in Fig. 8 that only the hystereses at the first excursions in each loading step have a feature similar to that under the unilateral loading. This is because under the circular orbit loading the column was first loaded only in the x direction in the first excursions at each loading step (refer to Fig. 2).

4 EFFECT OF LOADING ORBITS

Table 1 summarizes the maximum strengths and ultimate displacements. The ultimate displacements are defined here as the displacement where the strengths deteriorate to less than 80% of the maximum strengths. It is apparent that the strengths under the diagonal, square and circular orbit loadings are 10-20% smaller than those under the unilateral loading. The ultimate displacements under the diagonal, square and circular orbit loadings are 18-24% smaller than those under the unilateral loading.

Figs. 9, 10 and 11 compare the hystereses under the unilateral loading and those under the diagonal, square and circular orbit loadings. Since the hystereses under the diagonal, square and circular orbit loadings are similar between x and y directions, only the hystereses in the x-direction are presented here. The deterioration of strength, the pinching near zero displacements and the round corners near the peak displacements of the columns subjected to the diagonal, square and circular orbit loadings, respectively, are well predicted by the analysis.

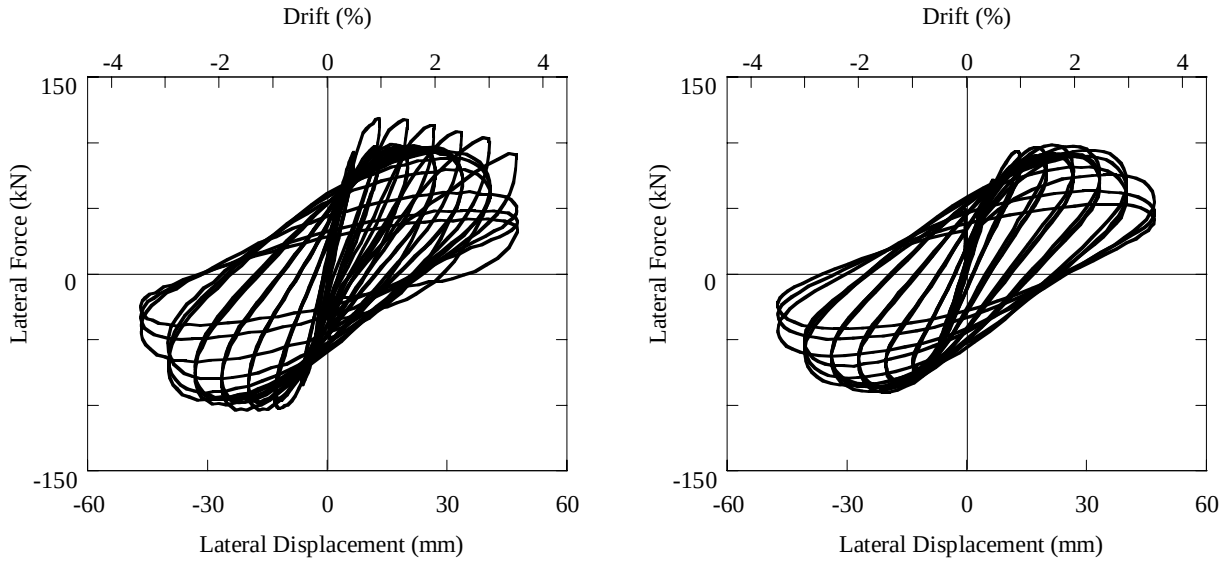

(a) x-Direction (b) y-Direction

(1) Circular Loading

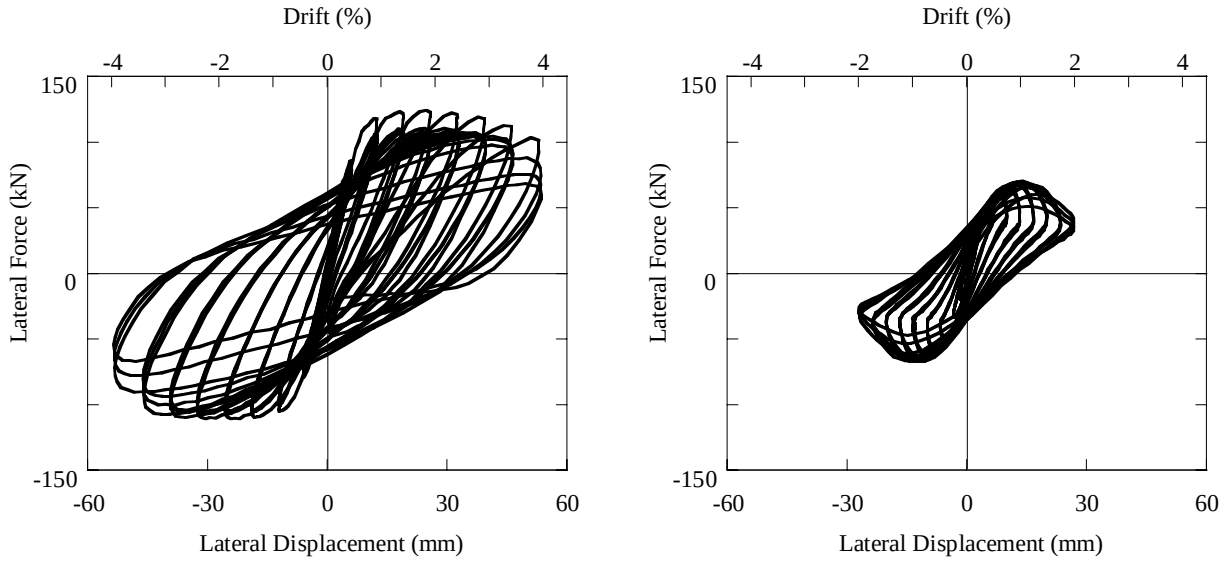

(a) x-Direction (b) y-Direction

(2) Ellipse Loading

Fig. 8 Lateral Force vs. Lateral Displacement Hystereses of Columns subjected to Circular Orbit Loading

5 FIBER ELEMENT ANALYSIS

5.1 Analytical Model

The columns were modeled as shown in Fig. 12. The plastic hinge zone was idealized by a fiber element. The effect of deformation of longitudinal bars in the footing was represented by a rotational szpring at the bottom of the columns. The stress σ_c vs. strain ε_c relation of the confined concrete was assumed based on Hoshikuma et al [1] as

$$\sigma_c = \begin{cases} E_c\varepsilon_c\left\{1-\frac{1}{n}\left(\frac{\varepsilon_c}{\varepsilon_{cc}}\right)^{n-1}\right\} & \cdots \quad 0 \le \varepsilon_c \le \varepsilon_{cc} \\ \sigma_{cc} - E_{des}(\varepsilon_c - \varepsilon_{cc}) & \cdots \quad \varepsilon_{cc} < \varepsilon_c < \varepsilon_{cu} \\ 0.2\sigma_{cc} & \cdots \quad \varepsilon_{cu} < \varepsilon_c \end{cases} \tag{1}$$

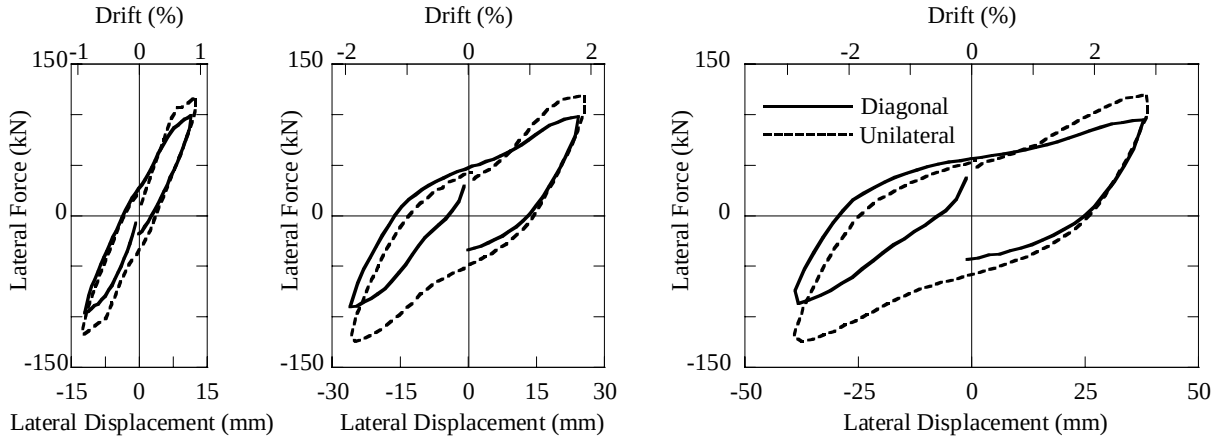

(a) Drift 1% (b) Drift 2% (c) Drift 3%

Fig. 9 Comparison of Hystereses between Columns subjected to Unilateral and Diagonal Orbit Loadings

Table.1 Effect of Bilateral Excitation

(a) Ultimate Strength

Loading Orbits	Maximum Flexural Strength (kN)						
	x-Direction			y-Direction			Average of (1) and (2)
	+	-	(1) Average	+	-	(2) Average	
Unilateral	119.8	124.5	122.2 (100%)	-	-	122.2 (100%)	122.2 (100%)
Diagonal	103.1	98.7	100.9 (83%)	100.6	88.3	94.5 (77%)	97.7 (80%)
Square	119.5	108.3	113.9 (93%)	109.3	101.6	105.5 (86%)	109.7 (90%)
Circular	118.8	103.5	111.2 (91%)	98.1	90.0	94.1 (77%)	103.2 (84%)
Ellipse	124.4	111.0	117.7 (96%)	-	-	-	-

(b) Ultimate Displacement

Loading Orbits	Ultimate Displacement (Drift)						
	x-Direction			y-Direction			Average of (3) and (4)
	+	-	(3) Average	+	-	(4) Average	
Unilateral	4.0	4.5	4.25 (100%)	-	-	4.25 (100%)	4.25 (100%)
Diagonal	3.5	3.5	3.5 (82%)	3.5	3.5	3.5 (82%)	3.5 (82%)
Square	3.0	3.5	3.25 (77%)	3.5	3.5	3.5 (82%)	3.38 (80%)
Circular	3.5	3.0	3.25 (77%)	3.5	3.0	3.25 (76%)	3.25 (76%)
Ellipse	4.0	4.0	4.0 (94%)	-	-	-	-

where, n: coefficient representing the shape of ascending branch, σ_{cc} and ε_{cc}: maximum strength of confined concrete and the strain corresponding to σ_{cc}, E_{des}: stiffness of confined concrete at the descending branch, ε_{cu}: ultimate strain, and they are represented as

$$n = \frac{E_c \varepsilon_{cc}}{E_c \varepsilon_{cc} - \sigma_{cc}} \tag{2}$$

$$\sigma_{cc} = \sigma_{ck} + 0.76 \rho_s \sigma_{sy} \tag{3}$$

$$\varepsilon_{cc} = 0.002 + 0.0132 \frac{\rho_s \sigma_{sy}}{\sigma_{ck}} \tag{4}$$

$$E_{des} = 11.2 \frac{{\sigma_{ck}}^2}{\rho_s \sigma_{sy}} \tag{5}$$

$$\varepsilon_{cu} = \varepsilon_{cc} + \frac{0.8 \sigma_{cc}}{E_{des}} \tag{6}$$

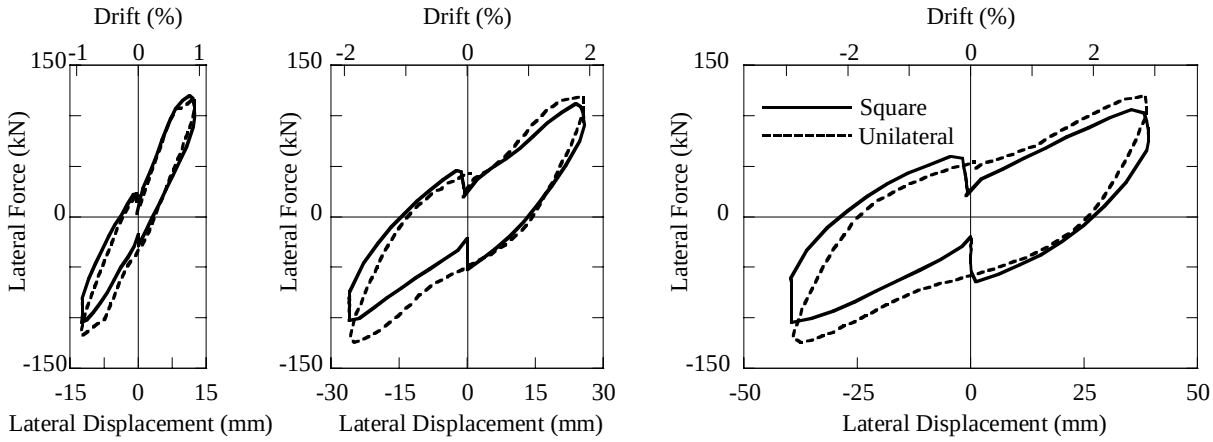

(a) Drift 1% (b) Drift 2% (c) Drift 3%

Fig. 10 Comparison of Hystereses between Columns subjected to Unilateral and Square Orbit Loadings

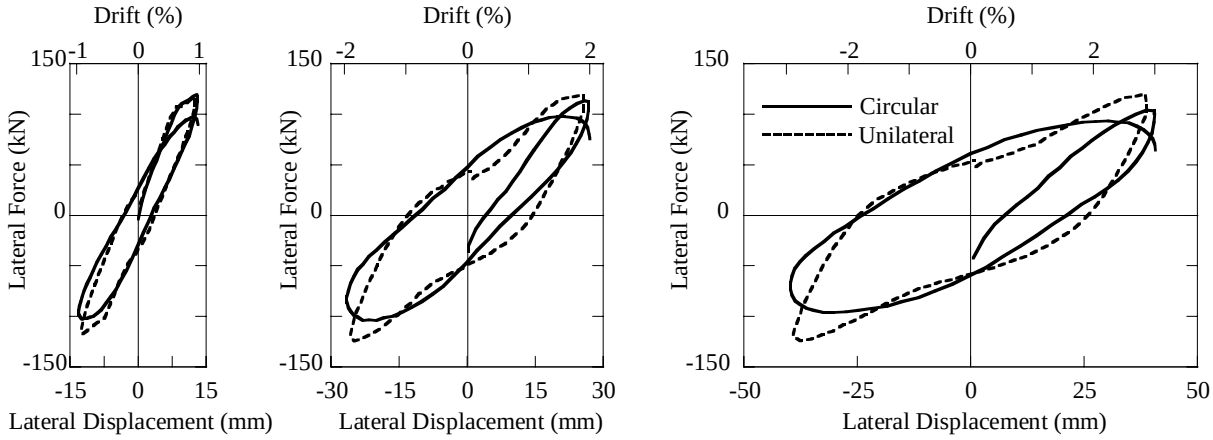

(a) Drift 1% (b) Drift 2% (c) Drift 3%

Fig. 11 Comparison of Hystereses between Columns subjected to Unilateral and Circular Orbit Loadings

where, σ_{ck} : strength of concrete, σ_{sy} : strength of tie bars, ρ_s : volumetric tie reinforcements ratio.

On the other hand, the stress σ_c vs. strain ε_c relation of the covering concrete was assumed as

$$\sigma_c = \begin{cases} E_c\varepsilon_c\left\{1-\dfrac{1}{n}\left(\dfrac{\varepsilon_c}{0.002}\right)^{n-1}\right\} & \cdots 0 \le \varepsilon_c \le \varepsilon_{cc} \\ \dfrac{\sigma_{cc}}{0.005}(0.007-\varepsilon_c) & \cdots\cdots \varepsilon_{cc} < \varepsilon_c \le \varepsilon_{cu} \\ 0 & \cdots\cdots \varepsilon_{cu} < \varepsilon_c \end{cases} \quad (7)$$

Unloading and reloading hystereses were idealized based on a model by Sakai, and Kawashima [2]. In this model, hystereses are provided for a set of 1) full unloading, 2) full reloading, 3) partial unloading and 4) partial reloading. For example, if a full unloading occurs from a point with strain ε_{ul} (unloading strain) on a skeleton curve, the strain reduces to $\varepsilon_{pl.1}$ at zero stress as shown in Fig. 13. This $\varepsilon_{pl.1}$ is called 1st plastic strain. Let $\sigma_{ul.1}$ represent the stress at ε_{ul} at the first unloading (1st unloading stress). If the concrete is reloaded from $\varepsilon_{pl.1}$ until the strain reaches the unloading strain ε_{ul}, the stress at this strain

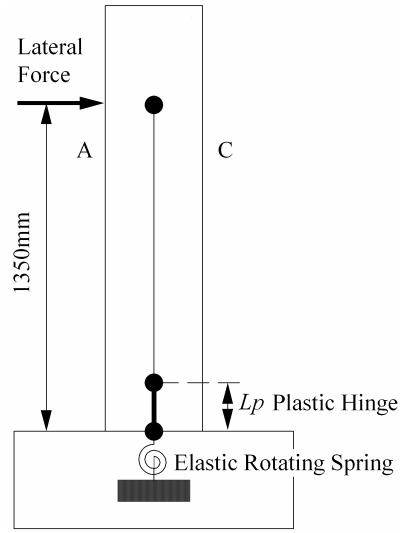

Fig. 12 Analytical Model

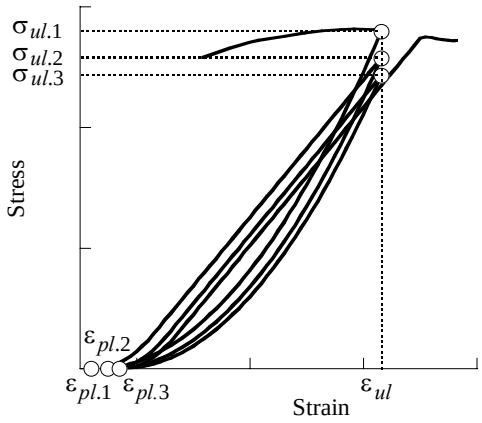

Fig. 13 Unloading and Reloading model of Confined Concrete

$\sigma_{ul.2}$ (2nd unloading stress) may be smaller than $\sigma_{ul.1}$. Thus, if we repeat a full unloading and a full reloading n times, the n-th unloading stress becomes $\sigma_{ul.n}$, and n-th plastic strain becomes $\varepsilon_{pl.n}$. The stress vs. strain relation of confined concrete subjected to n times full unloading and full reloading are represented as

$$\sigma_c = \sigma_{ul.n}\left(\frac{\varepsilon_c - \varepsilon_{pl.n}}{\varepsilon_{ul} - \varepsilon_{pl.n}}\right)^2 \tag{8}$$

$$\sigma_c = \begin{cases} 2.5\sigma_{ul.n}\left(\dfrac{\varepsilon_c - \varepsilon_{pl.n}}{\varepsilon_{ul} - \varepsilon_{pl.n}}\right)^2 & \cdots 0 \le \tilde{\varepsilon}_c < 0.2 \\ E_{rl}(\varepsilon_c - \varepsilon_{ul}) + \sigma_{ul.n+1} & \cdots 0.2 \le \tilde{\varepsilon}_c \le 1 \end{cases} \tag{9}$$

where, $\tilde{\sigma}_c$ and $\tilde{\varepsilon}_c$ are normalized stress and strain defined by

$$\tilde{\sigma}_c = \frac{\sigma_c}{\sigma_{ul.n}} \;;\; \tilde{\varepsilon}_c = \frac{\varepsilon_c - \varepsilon_{pl.n}}{\varepsilon_{ul} - \varepsilon_{pl.n}} \tag{10}$$

and E_{rl} represents the averaged stiffness in the reloading path between $0.2 \le \tilde{\varepsilon}_c \le 1$ defined by

$$E_{rl} = \frac{\sigma_{ul.n+1} - 0.1\sigma_{ul.n}}{0.8(\varepsilon_{ul} - \varepsilon_{pl.n})} \tag{11}$$

Representing the deterioration rate of $\sigma_{ul.n}$ and the increasing rate of $\varepsilon_{pl.n}$ by two parameters as

$$\beta_n = \frac{\sigma_{ul.n+1}}{\sigma_{ul.n}} \;;\; \gamma_n = \frac{\varepsilon_{ul} - \varepsilon_{pl.n}}{\varepsilon_{ul} - \varepsilon_{pl.n-1}} \tag{12}$$

β_n and γ_n are given as

For $n = 1,2$

$$\beta_n = \begin{cases} 1 & \cdots 0 \le \varepsilon_{ul} \le 0.001 \\ 1 - (10n + 22)(\varepsilon_{ul} - 0.001) & \cdots 0.001 < \varepsilon_{ul} < 0.0035 \\ 0.92 + 0.025(n-1) & \cdots 0.0035 \le \varepsilon_{ul} \le 0.03 \end{cases}$$

For $n \ge 3$

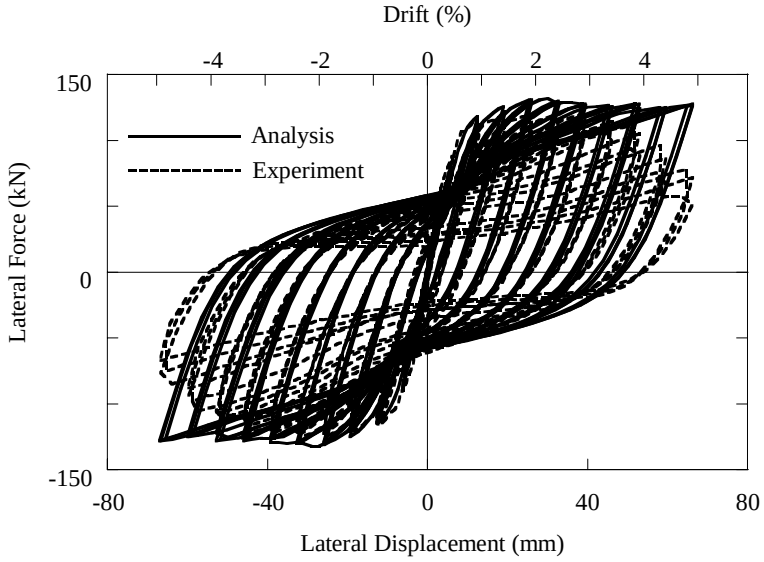

Fig. 14 Computed Lateral Force vs. Lateral Displacement Hystereses of a Column subjected to Unilateral Loading

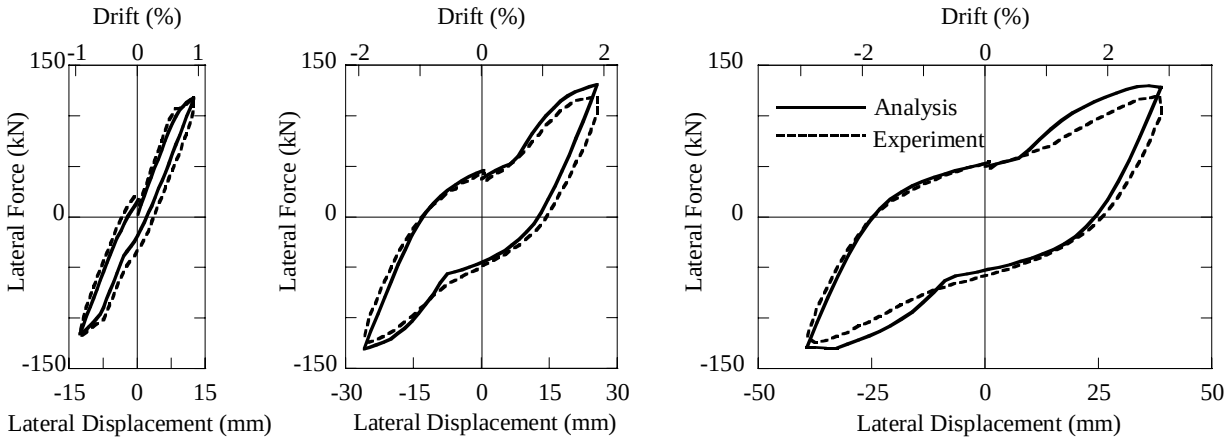

(a) Drift 1% (b) Drift 2% (c) Drift 3%

Fig. 15 Comparison of Analytical and Experimental Hystereses at 1%, 2% and 3% Drifts (Unilateral Loading)

$$\beta_n = \begin{cases} 1 & \cdots\cdots\ 0 \le \varepsilon_{ul} \le 0.001 \\ 1-(2n+8)(\varepsilon_{ul}-0.001) & \cdots\cdots\ 0.001 < \varepsilon_{ul} < 0.0035 \\ 0.965+0.005(n-3) & \cdots\cdots\ 0.0035 \le \varepsilon_{ul} \le 0.03 \end{cases} \quad (13)$$

$$\gamma_n = \begin{cases} 0.945 & \cdots n = 2 \\ 0.965+0.005(n-3) & \cdots n \ge 3 \end{cases} \quad (14)$$

On the other hand, the Menegotto-Pinto model was used to idealize the stress vs. strain hysteresis of the axial bars [3].

5.2 Analysis for Unilateral Loading

Fig. 14 compares the computed lateral force vs. lateral displacement hysteresis with the experimental result. Fig. 15 compares the hystereses in the first loading excursion of 1%, 2% and 3% drifts. The computed hystereses by the fiber element method are very close to the experimental results. Since the effect of local buckling and rupture of longitudinal bars is not

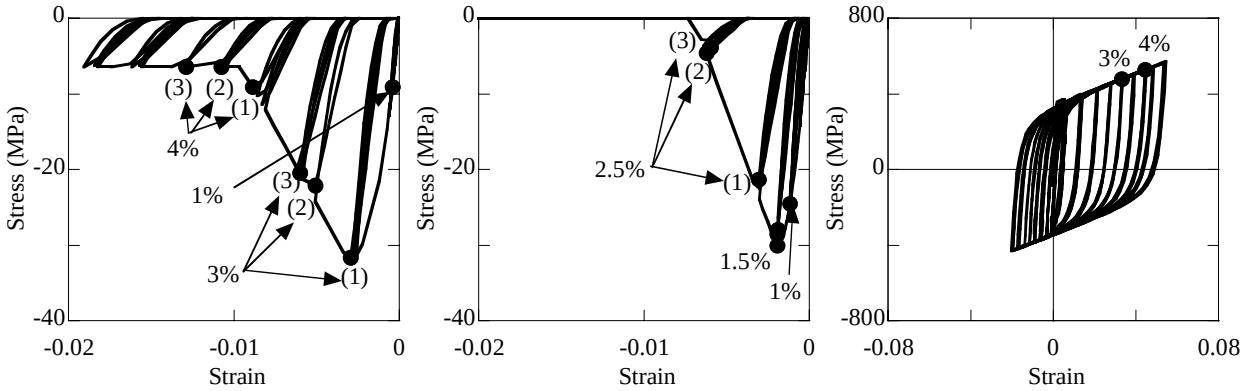

(a) Core Concrete (Extreme Fiber at A-Surface) (b) Covering Concrete (Extreme Fiber at A-Surface) (c) Longitudinal Bar (Center of A-Surface)

Fig. 16 Computed Stress vs. Strain Hystereses of a Column subjected to Unilateral Loading

included in the fiber element analysis, the hystereses after 3.5% drift are not accurately predicted.

Fig. 16 shows the computed stress vs. strain hystereses of the core concrete and the covering concrete at the extreme fibers and a longitudinal bar at the center of A surface (refer to Fig. 1). The stress of core concrete at the extreme fiber reaches the maximum strength σ_{cc} at the first loading excursion of 3% drift, and deteriorates to 20% of σ_{cc} at 4% drift. Because the covering concrete is not confined, stress of the covering concrete reaches the maximum strength σ_{cc} at 1.5 % drift, and becomes almost zero at the second excursion of 2.5% drift. Strain of the longitudinal bar becomes 0.033 at 3% drift and 0.045 at 4% drift.

The computed stress and strain of the core and the covering concrete and the longitudinal bar well represents the failure mode of the model column under the unilateral loading. The covering concrete started to spall off at 3% drift in the test. As described above, at this 3% drift it is predicted that the stress of covering concrete deteriorates to almost zero. Extensive failure of core concrete started to occur at 4% drift with the longitudinal bars and the ties being exposed in the test. At the 4% drift, it is predicted that the stress of the core concrete deteriorates to 20% of the maximum strength σ_{cc} in the analysis.

5.3 Analysis for Square Orbit Loading

Fig. 17 compares the lateral force vs. lateral displacement hystereses between the experiment and the analysis for x and y directions. The computed hystereses agree well with the experimental results until 3.5% drift. Over the 3.5% drift, the strength started to deteriorate significantly resulted from failure of not only the covering concrete but also the core concrete at all 4 surfaces in the test. Fig. 18 shows a comparison of the hystereses of the first excursion at 1%, 2% and 3% drifts between the test and the analysis. The sharp deterioration of the strength at the maximum and zero displacements are well predicted by the analysis.

Fig. 19 shows the computed stress vs. strain hystereses of the core and covering concrete at the extreme fibers and longitudinal bars at the center of the surfaces A and B (refer to Fig. 1). The hystereses at the A surface are similar to those at the B surface. At the extreme fiber of core concrete the stress reaches σ_{cc} at the 1st excursion of 2% drift, but it sharply deteriorates at the 3rd excursion. This shows that the core concrete starts to deteriorate extensively at 2% drift. At the extreme fiber of covering concrete the stress reaches σ_{cc} at 1.5% drift, and deteriorates to zero at the 3rd loading excursion of 2% drift. At the longitudinal bar at the center strain becomes 0.029 at 3% drift.

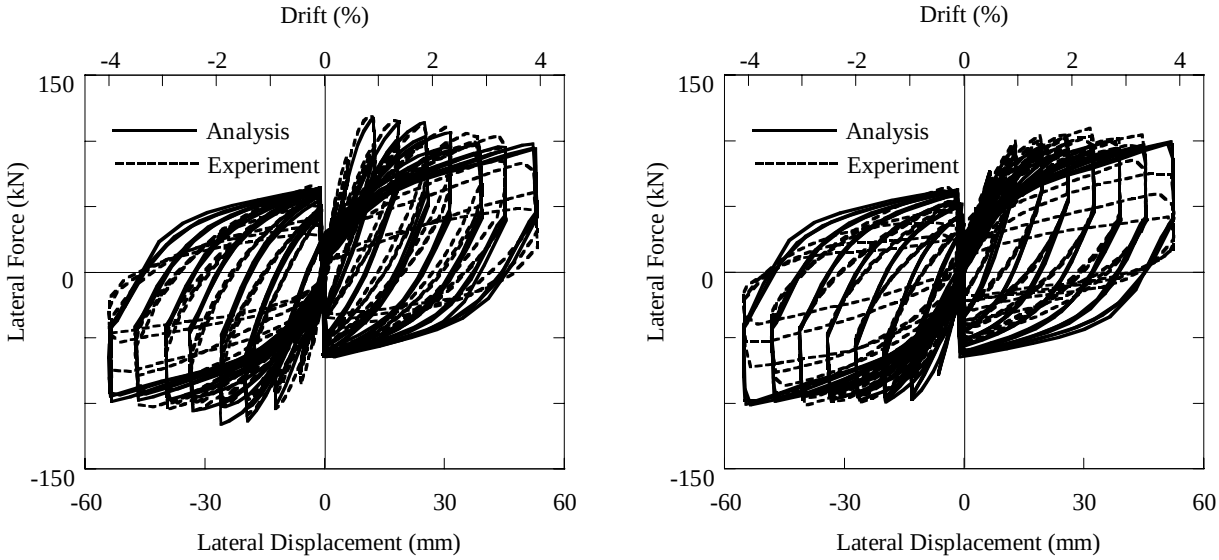

(a) x-Direction (b) y-Direction

Fig. 17 Computed Lateral Force vs. Lateral Displacement Hystereses of a Column subjected to Square Orbit Loading

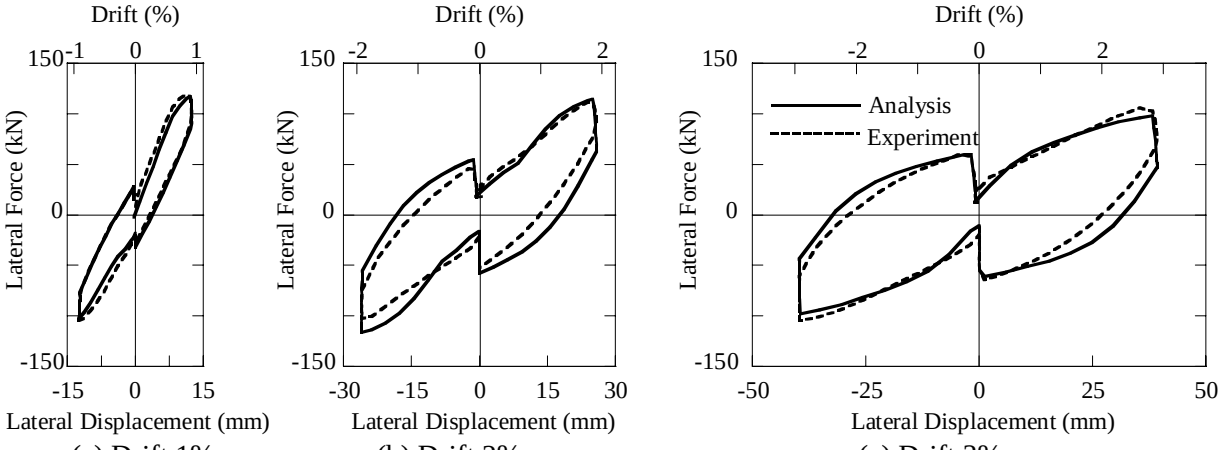

(a) Drift 1% (b) Drift 2% (c) Drift 3%

(1) x-Direction

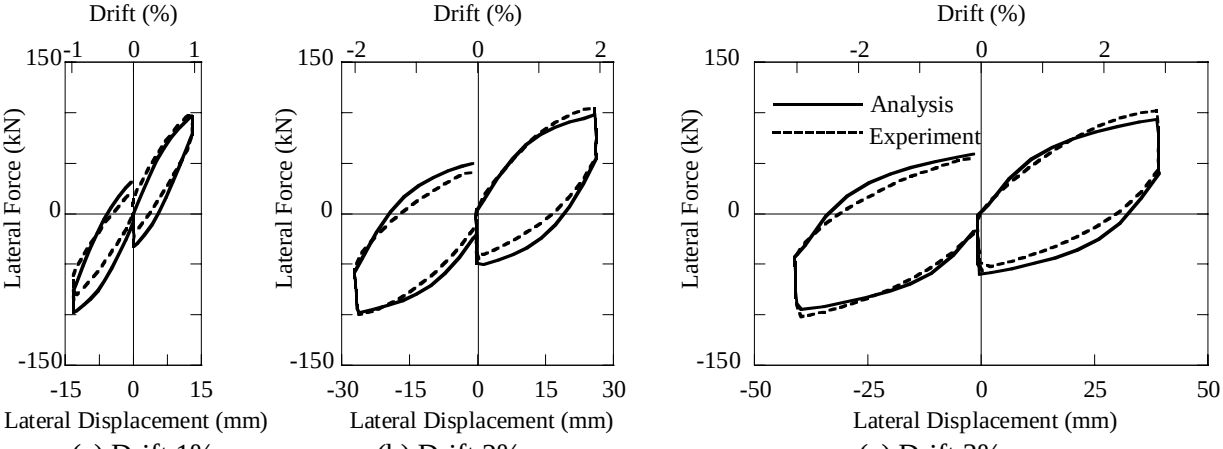

(a) Drift 1% (b) Drift 2% (c) Drift 3%

(2) y-Direction

Fig. 18 Comparison of Analytical and Experimental Hystereses at 1%, 2% and 3% Drifts (Square Orbit Loading)

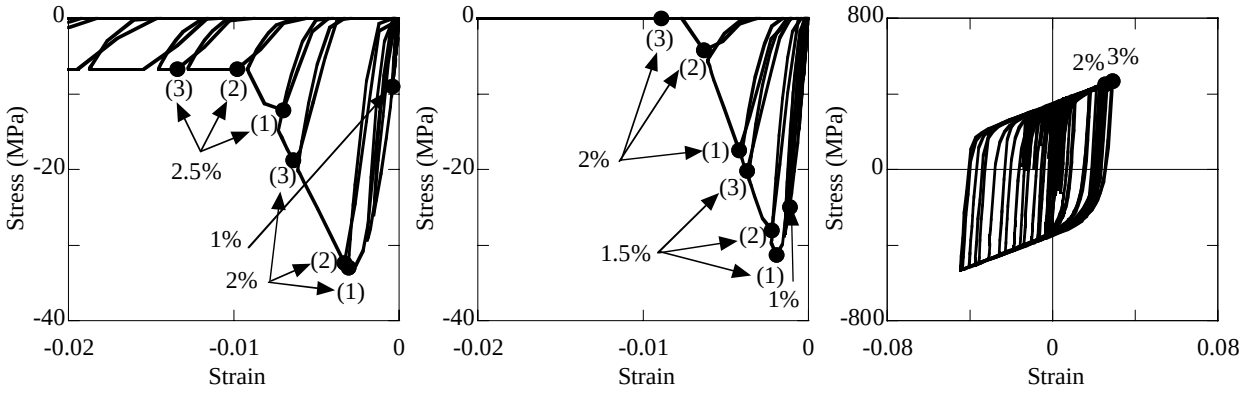

(a) Core Concrete (Extreme Fiber at A-Surface) (b) Covering Concrete (Extreme Fiber at A-Surface) (c) Longitudinal Bar (Center of A-Surface)

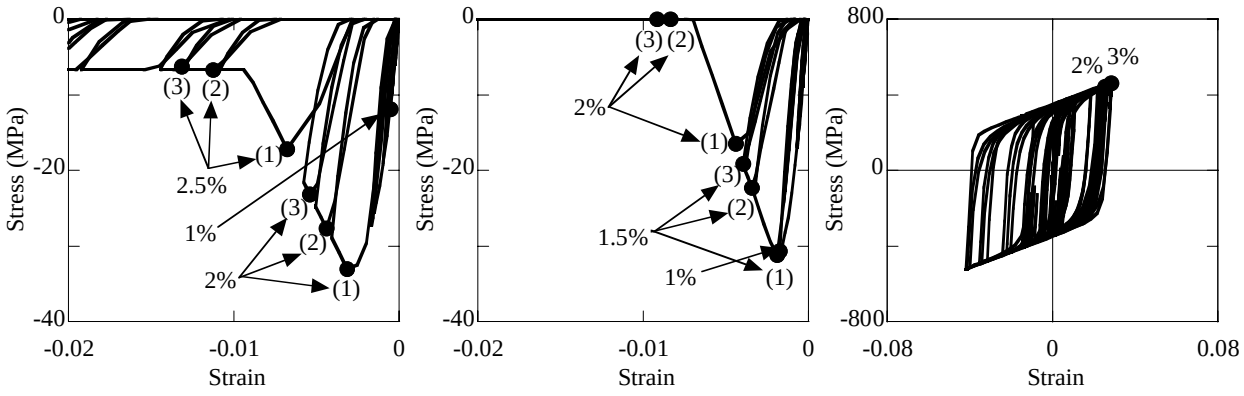

(a) Core Concrete (Extreme Fiber at B-Surface) (b) Covering Concrete (Extreme Fiber at B-Surface) (c) Longitudinal Bar (Center of B-Surface)

Fig. 19 Computed Stress vs. Strain Hystereses of a Column subjected to Square Orbit Loading (numbers in parentheses represent the number of loading excursions)

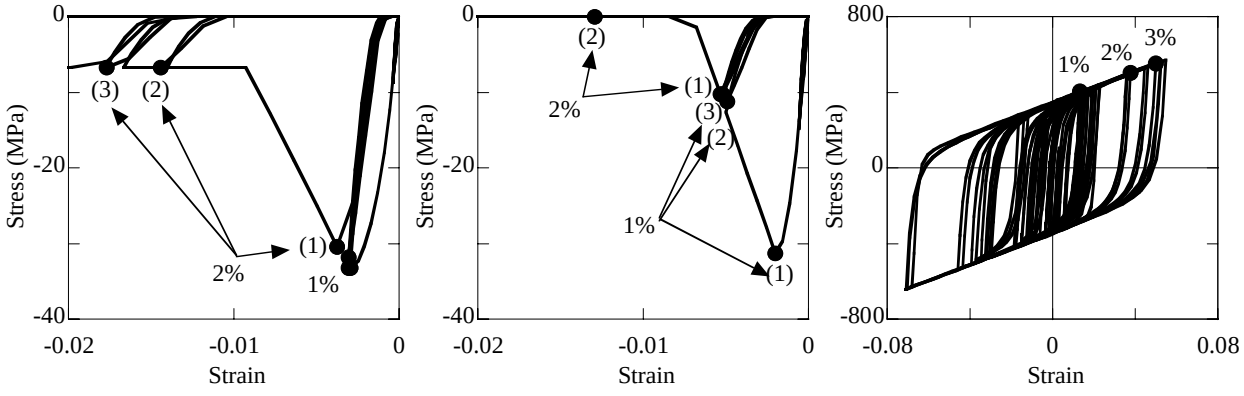

(a) Core Concrete (b) Covering Concrete (c) Longitudinal Bar

Fig. 20 Computed Stress vs. Strain Hystereses at the A-D Corner of a Column subjected to Square Orbit Loading

At the corners larger deterioration occurs resulted from the combination of bilateral excitation. Fig. 20 shows the computed stress vs. strain hystereses of the core and the covering concrete and the longitudinal bar at the A-D corner. It should be noted here that compressions of bilateral loading are coupled at 1%, 2% and 3% drifts at the A-D corner, but

they are not coupled here at 1.5%, 2.5% and 3.5% drifts. Due to the coupling of bilateral loading, the stress of core concrete reaches σ_{cc} at the first loading excursion of 1% drift. Although it is still 91% of σ_{cc} at the first loading of 2% drift, it sharply deteriorates to 20% of σ_{cc} at the second loading excursion of the 2% drift. The strain of the corner longitudinal bar is 0.05 at 3% drift, which is 72% larger than the strain of a longitudinal bar at the center of surface A. It is thus well explained that the corners are subjected to larger inelastic deformation. This, in turn, explains that the failure started to occur from the corners in the test.

6. CONCLUSIONS

A series of cyclic loading tests and a fiber element analysis were conducted to clarify the effect of bilateral loading of square reinforced concrete bridge columns. Based on the test and analysis presented herein, the following conclusions may be deduced.

1) Bilateral loading results in larger deterioration of flexural strength and ductility capacity of columns than that under the unilateral loading. In particular, this effect is significant under the square and circular orbit loadings.
2) Although failure started to occur at the surfaces in the plastic hinge zone subjected to alternative compression and tension under the unilateral loading, it started to occur from the corners under the bilateral loadings.
3) Fiber element analysis which takes account of deterioration of confined concrete predicts the test result with a good accuracy. The failure mode and progress of failure of the columns can be well explained based on the fiber element analysis.

7. ACKNOWLEDGEMENTS

The authors express their sincere appreciation to Dr. Yabe, M., Chodai Consultant, for design of the model columns, and Dr. Sakai, J., University of California, Berkeley, for use of the confined model of concrete. Extensive support was provided by Messrs. Uehara, K., Hatada, S., Yamagishi, M., Shimoyamada, E., Nakazawa, N., Nagata, S., Matsukawa, R., Wan, K. and Nakamura, G. for constructing and executing the cyclic loading test.

8. REFERENCES

1. Hoshikuma, J., Kawashima, K., Nagaya, K. and Taylor, A. W.: Stress-Strain Model for Confined Reinforced Concrete in Bridge Piers, Journal of Structural Engineering, ASCE, 123(5), 624-633, 1997
2. Sakai, J. and Kawashima, J.: An Unloading and Reloading Stress-Strain Model for Concrete Confined by Tie Reinforcements, Proc. 12th World Conference on Earthquake Engineering, CD-ROM No. 1432, Auckland, New Zealand, 2000.
3. Menegotto, M.and Pinto, P.E.: Method of Analysis for Cyclically Loaded R.C. Plane Frames Including Changes in Geometry and Non-Elastic Behavior of Elements under Combined Normal Force and Bending*, Proc. of IABSE Symposium on Resistance and Ultimate Deformability of Structures Acted on by Well Defined Repeated Loads*, pp.15-22, 1973